Acta Cryst. (1983). B39, 289–296

Structure and Planar Faults in the Defective NiAs-Type Compound $Ni_{17}S_{18}$

BY G. COLLIN AND C. CHAVANT

Laboratoire associé au CNRS n° 200, 4 avenue de l'Observatoire, 75006 Paris, France

AND R. COMÈS

Laboratoire de Physique des Solides, Associé au CNRS n° 2, Bâtiment 510, Université Paris-Sud, 91405 Orsay, France

(*Received* 22 *February* 1980; *accepted* 22 *November* 1982)

Abstract

Nickel sulphide, $Ni_{17}S_{18}$, is a vacancy-ordered superstructure $3a$–$3a$–$3c$ of the NiAs type. Its structure was solved using a microtwinned model with two types of domains with respective space groups $P3_121$ and $P3_221$; $a = 10{\cdot}290$ (2), $c = 15{\cdot}993$ (3) (Å), $R = 6{\cdot}4\%$ for 1122 reflections. The microtwinning mechanism corresponds to a glide vector (**a**–**b**)/3 in the substructure which is studied using Cowley's theory [Cowley (1976). *Acta Cryst.* A**32**, 83–87, 88–91]. The analysis of the diffuse streaks leads to a very weak fault rate ($\alpha = 0{\cdot}003$). The in-plane hexagonal Ni–Ni correlations are discussed.

1. Introduction

A great number of chalcogenides and pnictides of transition elements – especially $3d$ – crystallize in the hexagonal NiAs-type structure (Fig. 1) with two metallic atoms on the sixfold axis – z coordinate 0 and $\frac{1}{2}$ – and each of the two non-metallic atoms on a ternary axis alternately at $z = \frac{1}{4}$ and $\frac{3}{4}$. Owing to the presence of d elements these materials exhibit a wide range of magnetic, electronic or structural behaviour.

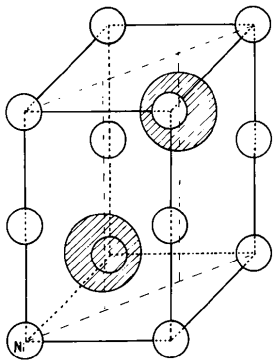

Fig. 1. Hexagonal NiAs-type cell. The large circles are As atoms and the small ones represent the metallic atoms.

Most of them also present extended domains of non-stoichiometry with respect to the ideal AB formula, either due to vacancies ($A_{1-x}B$), or to interstitial atoms (AA'_yB). This non-stoichiometry leads to the occurrence of very different kinds of superstructures and lattice distortions.

Among such compounds, nickel and iron sulphides both exhibit metal–non-metal transitions which are very sensitive to the composition. Indeed, the temperature and amplitude of the transition, the occurrence of hysteresis, magnetic anomalies and structural modifications strongly depend on small composition shifts.

Although the numerous superstructures of the iron compounds have been extensively studied, very little is known concerning nickel sulphide for which only one vacancy-ordered phase was reported by Barthelemy, Chavant, Collin & Gorochov (1976). The aim of the present paper, concerned with nickel sulphide, and of the following paper, dealing with iron sulphide (Keller-Besrest, Collin & Comès, 1983), is to show that, for these two sulphides, the phases containing a high concentration of vacancies (metallic region) present a common characteristic from the structural point of view: microtwins associated with stacking faults.

The theoretical framework for the study of stacking faults, which has been earlier elaborated by Jagodzinski (1949*a*,*b*,*c*, 1954), Kakinoki & Komura (1952, 1954*a*,*b*) and Kakinoki (1967), has received recently a new general approach proposed by Cowley (1976*a*,*b*) and Cowley & Au (1978) which allows analytical solutions for a great variety of stacking faults, including the most complex ones. We shall make use below of this theory referring to the papers by Cowley as Cowley I, II and III.

2. Average-structure determination

Powders of $Ni_{1-x}S$ were prepared from high-purity nickel (5N) previously reduced in hydrogen at 870 K and from distilled sulphur. Single crystals were grown by chlorine transport.

0108-7681/83/030289-08$01.50

The introduction of vacancies in NiS leads, for a composition close to $Ni_{0.94}S$, to the occurrence of a superstructure with hexagonal symmetry. The supercell dimensions are $3a$–$3a$–$3c$, where a and c refer to the NiAs subcell parameters (Barthelemy *et al.*, 1976). It is to be noted that the superstructure reflections are generally weak and that diffraction patterns obtained with usual filtered radiation do not reveal clearly the superstructure space group. In particular, no superstructure reflection can be detected along the 001 row because of the strong streaks due to the white radiation.

Using this limited data, a preliminary analysis of the vacancy ordering suggested a structure of space group $P6_3$ in which the equivalent positions were consistent with the atomic occupations of the NiAs-type structure. With this hypothesis the best result – after elimination of numerous weak superstructure reflections – yielded only a partial ordering of the vacancies.

Following these preliminary results, new series of diffraction experiments were performed with monochromatic radiation obtained from bent pyrolytic graphite. Under these improved conditions, it was possible to reveal a systematic extinction rule: the only $00l$ reflections present correspond to $l = 3n$. Moreover, a relationship between the intensities with $I_{hkl} = I_{hk\bar{l}} = I_{khl}$ suggests an apparent hexagonal symmetry.

This hexagonal symmetry, combined with the extinction condition, suggests a $P6_2$ space group for the superstructure (or the enantiomorphous $P6_4$). But this solution cannot be accepted. Indeed, a superstructure of the NiAs type cannot belong to one of these space groups, because they both have among their equivalent positions the relationship xyz and $\bar{x}\bar{y}z$, which is never simultaneously realized for nickel and sulphur atoms in the NiAs-type stacking (Figs. 1 and 2).

We were consequently led to adopt the solution earlier proposed by Fleet (1971) in order to resolve exactly the same type of difficulty in another NiAs vacancy-ordered superstructure: 'hexagonal' Fe_7S_8, of the $2a$–$2a$–$3c$ type. This solution consists of assuming that the observed hexagonal symmetry is only an apparent one due to the superposition on each Bragg peak of two independent reflections from microtwins. This hypothesis was recently confirmed by Nakano, Tokonami & Morimoto (1979).

Following these authors we note that it is possible to account for the whole set of observations using two trigonal space groups with, respectively, a 3_1 and a 3_2 axis, which is in agreement with the extinction condition $00l$ $l \neq 3n$. Among such groups, two are consistent with the NiAs-type stacking: $P3_1$ and $P3_121$ (and their two enantiomorphs $P3_2$ and $P3_221$). In order to employ the smallest number of variable parameters we adopted, in a first step, the $P3_121$ and $P3_221$ groups for which the relationship $I_{hkl} = I_{kh\bar{l}}$ is satisfied. With such a microtwinning the structure factors can be calculated as the square root of the sum $|F|^2_{hkl} + |F|^2_{hk\bar{l}}$.

The crystal used for the structural determination had a thickness of 50 μm and a largest in-plane dimension of 350 μm. Lattice constants determined by least-squares adjustment to the angular readings on an automatic four-circle diffractometer were $a = 10{\cdot}290$ (2) and $c = 15{\cdot}993$ (3) Å. They correspond to $a_s = 3{\cdot}430$ and $c_s = 5{\cdot}331$ Å for the NiAs-type substructure; these values reveal an appreciable contraction with respect to the high-temperature stoichiometric NiS with $a = 3{\cdot}441$ and $c = 5{\cdot}354$ Å (Barthelemy *et al.*, 1976). These lattice constants indicate a composition close to $Ni_{0.94}S$ as deduced from the dependence upon x of the lattice constants of $Ni_{1-x}S$.

1122 independent reflections were collected between $2\theta = 0$ and 65° (Mo $K\alpha$ radiation). They were first carefully corrected for the strongly anisotropic absorption due to the platelet shape of the crystal. The whole set of data was then introduced in the refinement

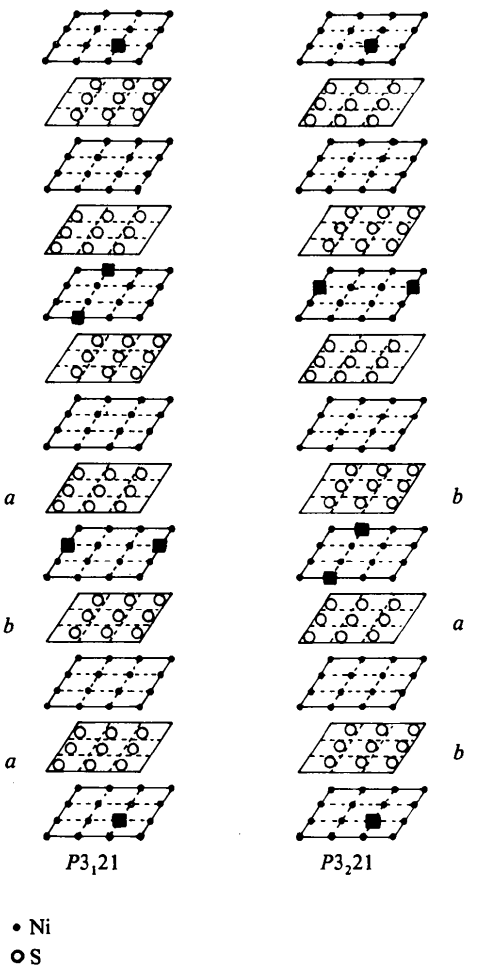

Fig. 2. Schematic representation of the vacancy ordering in the two domains of $Ni_{17}S_{18}$. The letters a and b refer to the types of sulphur planes as defined in §3.

including the 513 reflections with $I < \sigma$ (and 53 with $I = 0$). Among the 1122 independent reflections only 50 were exclusively due to the NiAs substructure.

The superstructure reflections with h and/or $k \neq 3n$ supply information on the superstructure. We noted that: (i) for hkl with $h \neq k$, the reflections with $l \neq 3n$ were the strongest; (ii) the reverse situation was observed for the hhl reflections; the strongest intensities were then found for $l = 3n$.

Finally the superstructure reflections along the substructure rows – hkl with h and $k = 3n$ and $l \neq 3n$ – were all weak.

Such an intensity distribution is consistent with the presence of three vacancies per unit cell on a 3(*a*) position of the $P3_121$ group (and on the equivalent position of $P3_221$) with ideal coordinates $\frac{1}{3},0,\frac{1}{3}$. In this case, indeed, non-zero intensity is only obtained (i) with $l \neq 3n$ for superstructure reflections with $h \neq k$ (and h or $k \neq 3n$); and (ii) with $l = 3n$ for $h = k \neq 3n$ superstructure reflections.

This corresponds to a formula $Ni_{0.944}S$ close to that deduced above from the lattice constants. On the basis of this good qualitative agreement, such a model was refined using $F_{hkl} = (F^2_{hkl} + F^2_{\bar{h}\bar{k}l})^{1/2}$. Convergence was obtained by starting with the ideal NiAs positions and with only two temperature factors, one for the nickel and one for the sulphur atoms. In a second step, individual temperature factors were attributed to each atom leading to a total of 72 variable parameters. Under these conditions the final R value was 6·4% for the whole set of reflections.

The separate R factors are 2·30% for the 50 substructure reflections and 10·40% for the 1072 superstructure ones (including the 513 with $I < \sigma$). With this great number of weak and very weak reflections this value of 10·40% can be considered as very satisfactory and establishes that the total R-factor value is not only due to the strong substructure reflections but includes the good agreement of the complementary superstructure reflections. As is usually observed for superstructure refinements, some correlations between atoms which are independent in the supercell but are bound by the substructure symmetry cannot be cancelled and introduce some rather large standard deviations with respect to a conventional structure determination (Table 1). This being said the observed deviations with respect to the ideal NiAs structure are perfectly significant as will be shown below.*

In a last step the consistency of the solution was tested: the different Ni occupation factors were systematically refined in order to evaluate the possible effects of correlations: first one by one; and successively in groups Ni(1), Ni(2), Ni(3) then Ni(4), Ni(5), Ni(6), finally Ni(7) to Ni(11).

Table 1. *Positional and thermal parameters in the $P3_121$ cell of $Ni_{17}S_{18}$*

	Number per unit cell	x	y	z	B (Å²)
Ni(1)	6	0·3328 (3)	−0·0004 (4)	0·0063 (1)	0·91 (3)
Ni(2)	6	0·6667 (3)	−0·0063 (5)	0·0004 (4)	0·94 (8)
Ni(3)	6	0·6676 (7)	0·3420 (6)	−0·0002 (2)	1·08 (6)
Ni(4)	6	0·3333 (4)	0·0009 (4)	0·1786 (1)	0·94 (2)
Ni(5)	6	0·6747 (6)	0·0093 (5)	0·1671 (4)	1·11 (8)
Ni(6)	6	0·6737 (9)	0·3337 (8)	0·1669 (1)	0·82 (6)
Ni(7)	3	0·0076 (9)	0	0·3333	0·94 (7)
Ni(8)	3	0·6593 (8)	0	0·3333	1·1 (1)
Ni(9)	3	0·0086 (8)	0	0·8333	0·76 (7)
Ni(10)	3	0·3339 (6)	0	0·8333	0·99 (3)
Ni(11)	3	0·6609 (6)	0	0·8333	0·8 (1)
Ni	0	0·3333	0	0·3333	
S(1)	6	0·1090 (11)	0·2235 (10)	0·0791 (6)	0·86 (9)
S(2)	6	0·4436 (10)	0·2221 (10)	0·0869 (4)	0·94 (9)
S(3)	6	0·7839 (9)	0·2246 (11)	0·0802 (4)	0·77 (9)
S(4)	6	0·1082 (12)	0·5526 (10)	0·0776 (5)	1·05 (9)
S(5)	6	0·4406 (9)	0·5549 (12)	0·0853 (5)	0·88 (8)
S(6)	6	0·7801 (11)	0·5546 (12)	0·0868 (4)	1·0 (1)
S(7)	6	0·1099 (8)	0·8878 (11)	0·0878 (5)	0·74 (8)
S(8)	6	0·4441 (12)	0·8890 (13)	0·0861 (5)	1·0 (1)
S(9)	6	0·7800 (11)	0·8942 (9)	0·0848 (4)	0·9 (1)

In neither case did any Ni atom occupancy reveal a deviation higher than the standard deviation of 0·02 and the R factor remained constant. All the Ni sites were then considered as completely filled. In the same way the occupancy of the 'vacant' Ni site was refined but quickly converged to zero.

This perfect ordering of the vacancies strongly confirms the twinned model and establishes that the formula of the 3*a*–3*a*–3*c* $Ni_{1-x}S$ compound is $Ni_{17}S_{18}$. The schematic repartition of atoms and vacancies in the two types of twins is shown in Fig. 2.

The same refinements were also performed with the $P3_1$ and $P3_2$ space groups in which the number of variable parameters is more than twice as large as for the $P3_121$ and $P3_221$ groups used above. Besides much higher standard deviations, the use of such groups did not lead to significant shifts with respect to the former results and the R factor was unchanged; consequently we rejected such an alternative description of the structure.

3. Stacking fault

Although other examples are known in the case of defective NiAs compounds it is nevertheless rather unnatural to refine with a twinned model, even if this does not introduce any additional variable parameters. In such a case the R-factor value alone does not constitute a sufficient justification of the model structure.

* A list of structure factors has been deposited with the British Library Lending Division as Supplementary Publication No. SUP 38249 (7 pp.). Copies may be obtained through The Executive Secretary, International Union of Crystallography, 5 Abbey Square, Chester CH1 2HU, England.

As no separation in the reflections was observed, even at high θ, we were led to adopt the hypothesis of a microtwin (which could also be deduced from the exact equivalence between unrelated reflections). This microtwin supposes a stacking fault. We shall see below that independent diffuse scattering measurements indeed confirm the existence of faults, and that the type of fault responsible for the diffuse scattering is further consistent with the microtwinned model used in the structure refinement.

Let us first define (Fig. 2) by type *a* the sulphur plane in which the sulphur atoms are close to the in-plane positions $x \simeq \frac{1}{3}$, $y \simeq \frac{2}{3}$ of the NiAs substructure (x, $y \simeq \frac{1}{9}, \frac{2}{9}, \ldots$ for the superstructure) and by *b* the sulphur plane of the second kind with sulphur atoms close to $x \simeq \frac{2}{3}, y \simeq \frac{1}{3}$ of the NiAs subcell.

Therefore, in the type-I twin ($P3_121$) of $Ni_{17}S_{18}$ a nickel plane with vacancies is always surrounded by an adjacent *a* sulphur plane at $z + \frac{1}{12}$ and by a *b* sulphur plane at $z - \frac{1}{12}$. In the type-II twin ($P3_221$) the reverse order is adopted, *b* sulphur plane with $z + \frac{1}{12}$ and *a* sulphur plane with $z - \frac{1}{12}$. Consequently, at the boundary between the two types of twins a fault is required in which one type of sulphur plane is changed into the other one.

The diffraction pattern of Fig. 3 reveals indeed very weak streaks directed along the *l* direction of reciprocal space and going through some of the strongest substructure reflections. For this reason we shall use below for simplification the NiAs-type subcell notation *a*–*a*–*c*.

A more precise examination of the diffuse pattern shows that such streaks are only observed along the rods with $h - k \neq 3n$, which go for instance through the strong Bragg reflections of the subcell such as 100, 101, 102, 200 and 202. No streaks are observed for rows with $h - k = 3n$, which also go through strong reflections of the subcell such as 300, 304, 002 and 004 for instance.

The intensity of the streaks is comparable to the intensity due to the thermal scattering coming from the small wave-vector acoustic phonons, which has the form of a broad maximum visible only around the strongest Bragg reflections with $h - k = 3n$ as well as with $h - k \neq 3n$. This gives an idea of the weakness of the intensity of the diffuse streaks, and of the overexposure needed in order to observe such streaks.

Since the streaks are in the *l* direction of reciprocal space, they indicate the existence of planar faults perpendicular to **c** in real space; their sharpness further shows that a large coherence length is retained within the hexagonal plane.

The distribution of such streaks or rods with $h - k \neq 3n$ allows further characterization of the nature of the planar fault. This is a situation similar to stacking faults in hexagonal close packing, and can be expressed by a glide vector $\mathbf{S} = \pm(\mathbf{a} - \mathbf{b})/3$ (**a**, **b** hexagonal lattice vectors) whose effect is to interchange the sixfold axis with either one or other threefold axis (Fig. 4). It is obvious that for this condition a slab with the structure factor F_1 will become after the fault $F_2 = F_1 \{\exp \pm 2\pi i \times (h\mathbf{a} - k\mathbf{b})/3\} = F_1$ if and only if $h - k = 3n$; in this case the amplitudes of the two successive planes add up, and contribute normally to the 3D diffraction only (no streaking). In all other cases F_1 will transform in $F_2 = F_1 \{\exp 2\pi i\varphi\}$ with φ depending upon h and k; only a fraction of the amplitudes of the two successive planes

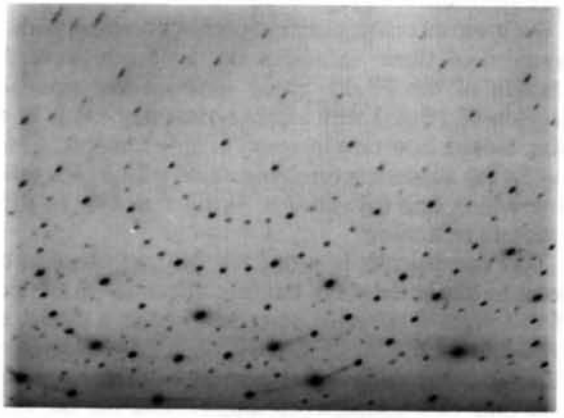

(*a*)

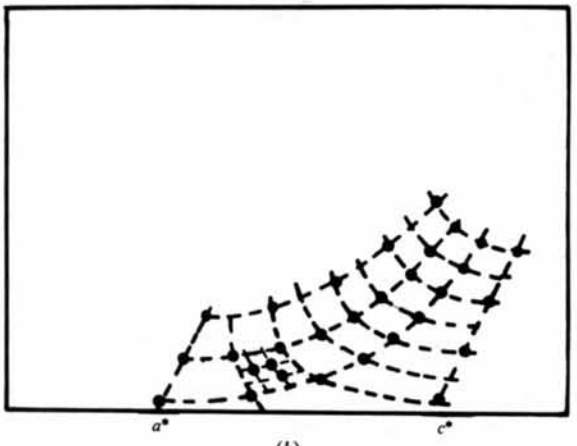

(*b*)

Fig. 3. (*a*) Diffraction pattern of the *h*0*l* layer of $Ni_{17}S_{18}$ (λ = Mo $K\alpha$, exposure time 10 d). (*b*) Substructure indexing of the NiAs reflections of Fig. 3(*a*). The indexing of the weak supplementary reflections can be found by dividing the a^* and c^* intervals by three as is shown on a small part of the reciprocal space.

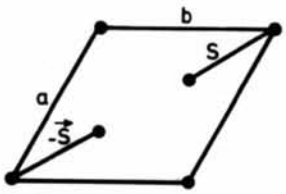

Fig. 4. Fault definition in the hexagonal plane of the NiAs-type substructure.

contributes to the usual 3D diffraction, the rest gives rise to the streaking.

With such a fault (Fig. 5*a*) a sulphur plane is of one type, say *b*, for the Ni before the fault and of the other type, say *a*, for the Ni after the fault as wished.

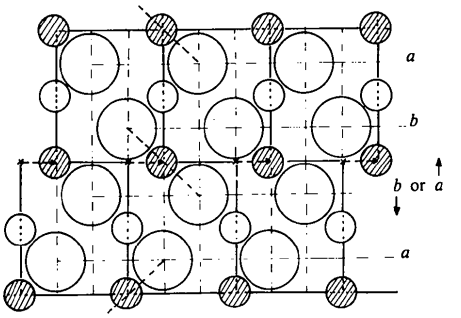

(*a*)

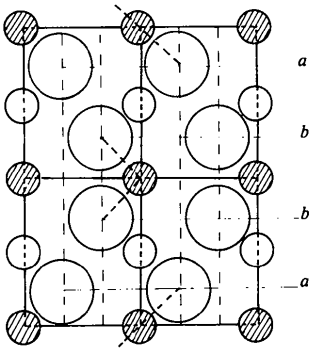

(*b*)

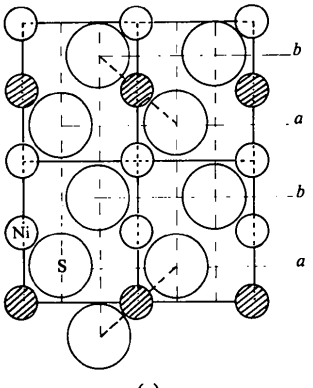

(*c*)

Fig. 5. Possible stacking faults compared with the experimental data in $Ni_{17}S_{18}$. Only model (*a*) gives satisfactory agreement. In the three cases the figures represent the (110) direct plane of the NiAs-type lattice. Large circles are S atoms and small ones are Ni atoms. The shaded Ni atoms belong to planes with vacancies. The letters *a* and *b* refer to the different sulphur-plane types of §3. (*a*) Glide vector (**a** − **b**)/3 interchanging the sulphur and nickel chains; (*b*) two superposed *b*-type sulphur planes; (*c*) fault in the vacancy stacking, instead of one Ni plane two are jumped before the next Ni plane with vacancies.

This distribution of the streaking intensities further allows elimination of the two other mechanisms which can also produce the change sulphur *a* ⇆ sulphur *b*.

(i) The hypothesis of a fault in the sulphur stacking such as two successive sulphur *a* (or *b*) planes, as shown in Fig. 5(*b*), would produce an increase of the *c* lattice constant at the fault. Two identical superposed sulphur planes would lead to a local *c* parameter of about 7·5 Å instead of the value of about 5·3 Å which is observed. This is the classical problem of planes which are displaced with respect to one another (Guinier, 1956) and would give a broadening of the reflections depending only upon *l*. Indeed such a fault would introduce phase shifts of the type exp $\{2\pi i l \Delta Z\}$ which do not depend upon *h* and *k* (no atomic shift in the plane) and would therefore affect reflections with the same *l* index in the same way. This is inconsistent with the observations showing the *h* and *k* dependence of the streaking.

(ii) The hypothesis of a fault concerning only the vacancy packing (Fig. 5*c*), a jump of zero or two unperturbed Ni planes between two Ni planes with vacancies. This would not produce streaking along the substructure rows because this is not a fault for the substructure: there is no modification with respect to the average packing of Ni and S atoms. Moreover, this would lead to a disordered distribution of vacancies between the independent Ni sites of the superstructure which is also inconsistent with the refinement.

We arrive therefore at the conclusion that the only consistent way to explain the streaking and the microtwinning mechanism is the glide plane of Fig. 5(*a*). The examination of the fault shows:

that it does not introduce any modification of the octahedral nickel surrounded by sulphur which accounts for the large in-plane correlations;

or, on the contrary, that one finds a modification of the sulpur surrounded by nickel, which at the fault becomes octahedral, while it is trigonal prismatic in a normal NiAs cell. In both cases, however, there are six Ni around each S atom, and this type of coordination for sulphur is commonly encountered in sulphides, even in the 3*d* series (in MnS for instance);

that one observes no modification of the vacancy stacking; each Ni plane with vacancies is surrounded, in the **c** direction, by two undisturbed Ni planes and *vice versa*, including the Ni plane at the fault.

To sum up, within the plane the fault only introduces minor changes and cannot be considered in any way as a deep perturbation of the structure. On the contrary, in the **c** direction its effect is to interchange the positions of the nickel and sulphur chains (but not the different atomic *z* coordinates) – and introduces some rather important perturbation which is again to be compared to the hexagonal close-packing fault which does not modify the planar correlations but interchanges vacant and occupied axes in the **c** direction.

4. Fault rate

In spite of the extreme weakness of the streaks we have tried to give a quantitative evaluation of the fault rate using Cowley's theory. As the streaking is roughly proportional to the reflection intensity and is hardly perceptible around the strongest substructure spots, it is perfectly logical that nothing is observed around the weak superstructure reflections (though in principle the streaking must also exist). This justifies the use of the substructure approximation in the calculation. We start from the simplified equation of diffraction [Cowley I, formula (9) (case $\sum_i G_i = 0$)], and use two translation vectors $\mathbf{S}_1 = -\mathbf{S}_2 = \mathbf{S} = (\mathbf{a} - \mathbf{b})/3$, two types of structure factors $F_1 = F_{hkl}$ and $F_2 = F_{hk\bar{l}} = -F_{hkl}$, $g_1 = g_2 = \frac{1}{2}$ (microtwin), $\mathbf{u}$ and $\mathbf{R}$ respectively for reciprocal- and direct-lattice propagation vectors, and 2α because two equally probable faults are considered. The Cowley equation is then written

$$I/N = \frac{F^*}{f}\left\{F + \frac{\alpha A}{f}\left[-F + \frac{\alpha A}{f} \times (F + \ldots)\right]\right\} + \text{c.c.} - |F|^2 \qquad (1)$$

$$f = 1 - (1 - 2\alpha)\exp\{2\pi i\, \mathbf{u}.\mathbf{R}\}$$

$$A = \exp\{2\pi i\, \mathbf{u}.\mathbf{R}\} \times \Sigma$$

with

$$\Sigma = 2\cos\{2\pi(h - k)/3\}.$$

We have solved this equation and neglecting the added and subtracted planes this gives

$$\begin{aligned} I/N = |F|^2 \Big\{ & 1 - [(1 - 2\alpha)^2 - (\alpha\Sigma)^2]^2 \\ & + 4(1 - 2\alpha)\alpha\Sigma \\ & - 2\cos\{2\pi\,\mathbf{u}.\mathbf{R}\}(1 - 2\alpha) \\ & \times [1 + (\alpha\Sigma)^2 - (1 - 2\alpha)^2] \\ & + 2\cos\{2\pi\,\mathbf{u}.\mathbf{R}\}(\alpha\Sigma) \\ & \times [(\alpha\Sigma)^2 - (1 - 2\alpha)^2 - 1]\Big\} \\ & \times \Big\{ 1 + [(1 - 2\alpha)^2 - (\alpha\Sigma)^2]^2 + 4(1 - 2\alpha)^2 \\ & + 4\cos\{2\pi\,\mathbf{u}.\mathbf{R}\}(1 - 2\alpha) \\ & \times [(\alpha\Sigma)^2 - (1 - 2\alpha)^2 - 1] \\ & + 2\cos\{2\pi\,\mathbf{u}.2\mathbf{R}\} \\ & \times [(1 - 2\alpha)^2 - (\alpha\Sigma)^2]\Big\}^{-1}. \end{aligned}$$

It is to be noted that this calculation leads to the value $(1 - 2\alpha)/2\alpha$ in the limit of $\cos(2\pi\,\mathbf{u}.\mathbf{R}) \to 1$ for the unperturbed reflections with $h - k = 3n$ as should be expected in this type of stacking fault (Cowley I).

With the formula one verifies that no streaking occurs on the $h - k = 3n$ rows and more generally that the calculated diffraction function is in agreement with the observed pattern. The biggest problem for the fault-rate determination is the scaling of the diffuse streaks with respect to the main reflection intensities from which they are issued and which are always completely saturated when the former are observed. The calibration can only be obtained indirectly through the intensities of weak surrounding superstructure reflections. Under these conditions it was possible to analyse the long streak around the 100 substructure reflection for which the perturbation by the superstructure reflections is imperceptible. The experimental curve was established over one hundred data points between 100 and 101 using an automatic Optronics microdensitometer.

It is verified that, starting from a weak enough fault rate, the curve shape given by the equation depends only weakly on α. In addition, it gives systematically the characteristic drop to zero intensity around $l \simeq 0{\cdot}50$ with an intensity divided by two per l intervals of one tenth in agreement with the observations. An α value of 0·003 gives a streak for which the intensities are in the good ratio with the integrated intensities of the superstructure reflections – and gives the calculated curve of Fig. 6.

This fault rate is very weak and corresponds to a fault about every 800 Å on an average, that is to say at the limit of detectability. This low rate explains why it is necessary to use strictly monochromatic radiation in order to be able to observe it. This very low rate also explains why a refinement with two scale factors, one for the substructure reflections and the second for the superstructure ones did not give significant shifts between the two: the coherence length is in the same range for the two types of reflections. This justifies the use of only one scale factor for the overall structure.

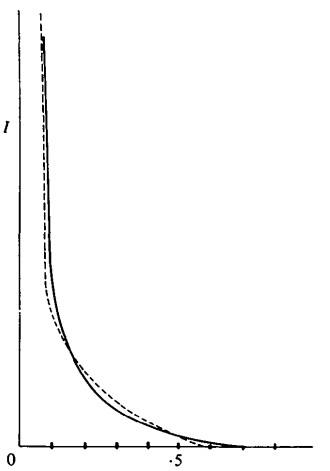

Fig. 6. Observed (full line) and calculated (dashed curve) with α = 0·003 diffraction functions.

5. Discussion

Since both the usual structural refinement and the less-common analysis of the faults described above give consistent results which support our microtwinned model, we shall discuss below in more detail the resulting $3a$–$3a$–$3c$ superstructure which has not previously been observed in NiAs-type compounds.

As is well known, the occurrence of vacancies in defective NiAs-type compounds can lead to a superstructure in which the interatomic distances between the metal atoms are significantly shorter compared to those observed in the reference-average subcell (see for instance Fe_7S_8). In order to emphasize the very special role played by the sites belonging to the chains which contain vacancies, we shall examine separately the interatomic distances along the hexagonal axis **c** and within the hexagonal plane. The distances observed in $Ni_{17}S_{18}$ will be compared to the corresponding distances in the subcell of the reference NiAs-type structure, that is to say $a = 3{\cdot}43$ and $c = 5{\cdot}33$ Å.

(*a*) In this ideal subcell each Ni atom is surrounded by two other Ni atoms, at a distance of 2·66 Å ($c/2$), on the sixfold axis. In the $3a$–$3a$–$3c$ superstructure there are nine chains each with six Ni sites in the **c** direction (Fig. 2): three chains with Ni(1), Ni(4)–Ni(10) and Ni□, three chains with Ni(2), Ni(5), Ni(8) and Ni(11), two chains with Ni(3) and Ni(6), one chain with Ni(7) and Ni(9).

The most important variations are observed on the chains containing the vacant Ni□ site (Fig. 7*a*). The two Ni(4) atoms surrounding the vacancy are strongly displaced towards this vacant site with Ni(4)–Ni□ distances of 2·48 Å. This leads to an important relaxation of the other Ni–Ni distance on the same chains which range between 2·75 and 2·77 Å (all standard deviations are smaller than 0·02 Å). This is obtained by the Ni(1) displacement toward the vacant site too, leaving the Ni(10) position unchanged with respect to the substructure. For this chain the average Ni–Ni distance [including Ni(4)–Ni□] is 2·66 Å, that is to say the ideal substructure value.

On the other hand, along the same **c** direction but for the six other chains which do not contain vacancies, the Ni–Ni distances remain close to the average value: between 2·66 and 2·68 Å.

(*b*) In the hexagonal planes the most significant modifications are again associated with the four sites of the perturbed chains Ni(1), Ni(4), Ni(10) and Ni□. Let us recall that in the ideal subcell each Ni atom would be surrounded by six Ni atoms at a distance of 3·43 Å (the subcell a parameter). In $Ni_{17}S_{18}$ two situations are to be considered (Figs. 7*b* and 7*c*):

(i) Around the two undisplaced special positions Ni(10) and Ni□ short distances with respect to the reference subcell are observed not only between these two sites and the six surrounding Ni atoms but also between the surrounding Ni atoms themselves. These distances all range from 3·35 to 3·37 Å (Figs. 7*b* and 7*c*).

(ii) On the other hand, around the two displaced general positions Ni(1) and Ni(4) the six Ni–Ni distances are larger than the average between 3·47 and 3·49 Å.

Consequently, we shall define the Ni–Ni correlations in the $3a$–$3a$–$3c$ superstructure as hexagonal: all the Ni atoms, with the exception of Ni(1) and Ni(4) are situated on hexagons with either Ni(10) or Ni□ in the centre; these small hexagons are non-adjacent, each one being surrounded by six large hexagons centred on either Ni(1) or Ni(4). This is the first time that this hexagonal correlation has been described in NiAs-type compounds.

The surrounding of the other Ni atoms is the consequence of the previously mentioned correlation; each of them [Ni(2), Ni(3), Ni(5), Ni(6), Ni(7), Ni(8), Ni(9), Ni(11)] exchanges: three short distances ($3{\cdot}35 < d < 3{\cdot}37$ Å) with the hexagon centre [Ni(10) or Ni□], and with the two adjacent Ni atoms of the same hexagon; three long distances among which two are with the perturbed Ni(1) or Ni(4) atoms (between 3·46 and 3·48 Å) and the third which is very large (3·58–3·59 Å) with a Ni of another hexagon.

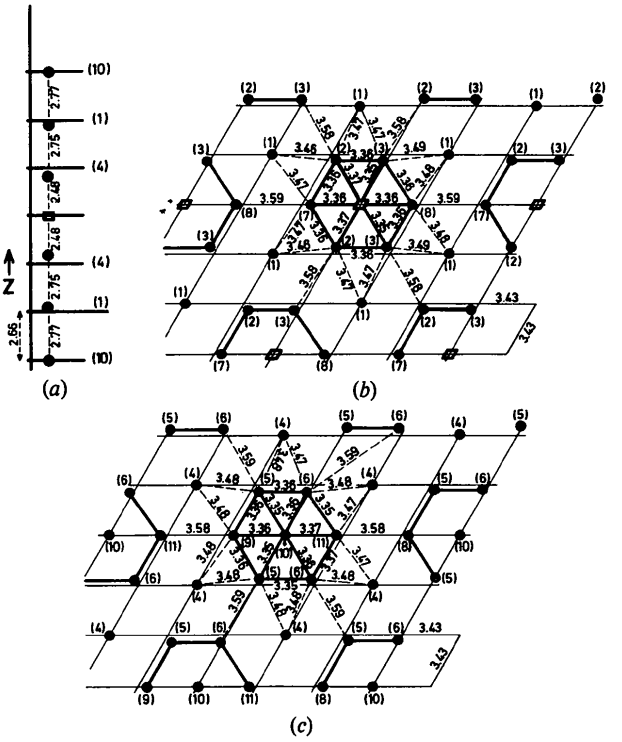

Fig. 7. Ni–Ni correlations (the numbers within brackets refer to the Ni atoms as defined in Table 1). (*a*) Ni–Ni correlations along the **c** axis for the Ni chains containing vacancies; (*b*) Ni–Ni correlations in the nickel planes with vacancies ($z = \frac{1}{3}$); (*c*) Ni–Ni correlations in the nickel planes without vacancies ($z = \frac{5}{6}$).

One can note that, in general, the observed displacements in $Ni_{17}S_{18}$ relative to the ideal positions in the reference NiAs subcell are rather small; this contrasts with the larger displacements observed, for instance, for the superstructure in $Fe_{1-x}S$. Such small displacements further explain the weaker superstructure reflections of $Ni_{17}S_{18}$ and the greater difficulties encountered for their experimental recording (the need of monochromatic radiation is more common for diffuse scattering than for Bragg reflections).

Finally, in the ideal subcell each Ni atom would be in the centre of an octahedron with six Ni–S distances equal to 2·39 Å. In $Ni_{17}S_{18}$ the average Ni–S distances are in the same range (2·37 to 2·40 Å); the smallest and largest individual distances are respectively 2·30 and 2·48 Å. These last distances both occur in the surrounding of the strongly displaced Ni(4) atom, while the distances with the vacant Ni site are normally relaxed (2·44 Å on average).

6. Conclusion

The structure of the first vacancy-ordered compound described in the $Ni_{1-x}S$ system can be solved using a microtwinned model which respects at the same time the observed extinction condition and the fundamental NiAs-type stacking of nickel and sulphur atoms. The validity of the model is established first by the satisfactory value of the R factor obtained in the refinement and also by the analysis of the stacking fault responsible for the microtwinning. In these conditions the complete structure is described at the same time in its ordered aspects as well as in its disordered ones.

References

BARTHELEMY, E., CHAVANT, C., COLLIN, G. & GOROCHOV, O. (1976). *J. Phys (Paris) Colloq.* **4**, 17–22.

COWLEY, J. M. (1976*a*). *Acta Cryst.* A**32**, 83–87.

COWLEY, J. M. (1976*b*). *Acta Cryst.* A**32**, 88–91.

COWLEY, J. M. & AU, A. Y. (1978). *Acta Cryst.* A**34**, 738–743.

FLEET, M. E. (1971). *Acta Cryst.* B**27**, 1864–1867.

GUINIER, A. (1956). *Théorie et Technique de la Radiocristallographie.* Paris: Dunod.

JAGODZINSKI, H. (1949*a*). *Acta Cryst.* **2**, 201–207.

JAGODZINSKI, H. (1949*b*). *Acta Cryst.* **2**, 208–214.

JAGODZINSKI, H. (1949*c*). *Acta Cryst.* **2**, 298–304.

JAGODZINSKI, H. (1954). *Acta Cryst.* **7**, 17–25.

KAKINOKI, J. (1967). *Acta Cryst.* **23**, 875–885.

KAKINOKI, J. & KOMURA, Y. (1952). *J. Phys. Soc. Jpn*, **7**, 30–36.

KAKINOKI, J. & KOMURA, Y. (1954*a*). *J. Phys. Soc. Jpn*, **9**, 165–176.

KAKINOKI, J. & KOMURA, Y. (1954*b*). *J. Phys. Soc. Jpn*, **9**, 177–183.

KELLER-BESREST, F., COLLIN, G. & COMÈS, R. (1983). *Acta Cryst.* B**39**, 296–303.

NAKANO, A., TOKONAMI, M. & MORIMOTO, N. (1979). *Acta Cryst.* B**35**, 722–724.

Acta Cryst. (1982). B**38**, 296–303

Structure and Planar Faults in the Defective NiAs-Type Compound 3*c* Fe_7S_8

BY F. KELLER-BESREST AND G. COLLIN

Laboratoire associé au CNRS n° 200, 4, avenue de l'Observatoire, 75006 Paris, France

AND R. COMÈS

Laboratoire de Physique des Solides, Associé au CNRS n° 2, Bâtiment 510, Université Paris-Sud, 91405 Orsay, France

(*Received* 22 *February* 1980; *accepted* 22 *November* 1982)

Abstract

The structure of 3*c*-type iron sulphide, Fe_7S_8, grown by vapour transport was re-examined; $a = 6·866$ (1), $c = 17·088$ (2) Å. The R factor obtained with the microtwinned model is 4·25% for 573 reflections. The incomplete ordering of the vacancies is explained by the occurrence of about 20% 4*c* sequences in the overall 3*c* lattice. The quantitative analysis of the diffuse streaks using Cowley's theory allows the interpretation of the microtwinning mechanism as a translation vector $\pm$ (**a** – **b**)/6 in the superstructure cell. The calculated fault rate is equal to 0·03.

1. Introduction

Numerous structural studies have already been devoted to the various NiAs-type phases encountered in the $Fe_{1-x}S$ system. Many of them were performed on natural crystals and a great number of superstructures of the main NiAs-type lattice have been found. In

0108-7681/83/030296-08$01.50